
# Process Planning for Additive Manufacturing of Geometries with Variable Overhang Angles using a Robotic Laser Directed Energy Deposition system

Farzaneh Kaji , Arackal Narayanan Jinoop , Mark Zimny , German Frikel , Kyle Tam , Ehsan Toyserkani

PII: S2772-3690(22)00010-X
DOI: https://doi.org/10.1016/j.addlet.2022.100035
Reference: ADDLET 100035

To appear in: *Additive Manufacturing Letters*

Received date: 5 January 2022
Revised date: 27 January 2022
Accepted date: 30 January 2022

Please cite this article as: Farzaneh Kaji , Arackal Narayanan Jinoop , Mark Zimny , German Frikel , Kyle Tam , Ehsan Toyserkani , Process Planning for Additive Manufacturing of Geometries with Variable Overhang Angles using a Robotic Laser Directed Energy Deposition system, *Additive Manufacturing Letters* (2022), doi: https://doi.org/10.1016/j.addlet.2022.100035

## Highlights

- Process planning for LDED-PF with overhang features is computationally extensive and it requires extensive pre-process considerations
- Full 5-axis method to fabricated LDED-PF parts is complicated due to collision happening between the deposition head and previously built layers
- 3+2 techniques show surface irregularities during the fabrication of LDED-PF parts in the transition regions
- In this research, we presented a novel approach to fabricate a hemisphere dome with variable overhang features in two directions using full 5-axis technique continuously with enhanced surface finish comparing to 3+2 technique

# Process Planning for Additive Manufacturing of Geometries with Variable Overhang Angles using a Robotic Laser Directed Energy Deposition system

Farzaneh Kaji[1,2,*] Arackal Narayanan Jinoop [1,2], Mark Zimny[2], German Frikel[3], Kyle Tam[1,], Ehsan Toyserkani[1]

[1] *Multi-Scale Additive Manufacturing Lab, Department of Mechanical and Mechatronics Engineering, University of Waterloo, Waterloo, ON N2L 3G1, Canada*.

[2] *Promation, 2767 Brighton Rd, Oakville, ON L6H 6J4, Canada.*

[3] *ModuleWorks GmbH, Henricistraße 50, 52072, Aachen, Germany*

**Corresponding author: farzaneh.kaji@gmail.com*

**Abstract**

In the present work, a novel Laser Directed Energy Deposition (LDED) process planning methodology is proposed to build a dome structure with variable overhang angles. Overhang structures with different overhang angles were built where the maximum angle of 35° can be used to build overhang structures without the process and structure compromise. The thin-wall hemispherical dome built using the developed methodology shows the maximum deviation of 2% with respect to the diameter of the original CAD model data. The study paves a way for building high-value, lightweight thin-walled structures with complex cylindrical-based shape (e.g., storage tanks, nozzles, combustion chambers) for engineering applications.

**Keywords:** Laser Directed Energy Deposition; Process Planning; Tool path generation; Overhang geometry; Additive manufacturing.

## 1. Introduction

Metal Additive Manufacturing (MAM), a disruptive technology, is revolutionizing industrial manufacturing through a unique combination of shape and material design freedom [1–3]. MAM enable the fabrication of lightweight and complex shaped structures, which requires process-

specific planning and strategy development. Laser Directed Energy Deposition (LDED), a class of MAM processes, possesses the ability to build the components with free-from geometry by injecting feedstock material directly into the melt-pool created on the surface of substrate/ previously built layer using a laser source. LDED systems often use three-axis or five-axis configuration to build intricate components. However, increasing focus on the deployment of five-axis configuration is seen recently due to improved freedom to build complex shaped components with overhang feature[4–6]. The five-axis configuration allows the nozzle to remain tangent to the surface, which elimiates the need for support structures to build features having a larger overhang angle (α) [7]. However, this configuration increases the process complexity and probability of collision between the nozzle and substrate/ previously deposited layers. It is not advisable to have collisions that can damage the LDED nozzles as they are costly and collision sensitive. In addition, focusing on the overhang features is a critical matter for the LDED and extrusion processes. The evaluation of the maximum overhang angle ($\alpha_{max}$) is critical and once the $\alpha$ exceeds the maximum limit, the structure collapses due to a lack of force balance between gravitational forces, surface tension, and capillary forces[8].

Researchers have investigated the fabrication of thin-wall structures with overhang features such as dome structures, which is challenging primarily due to the continuously changing $\alpha$ in two directions and chances of collision between the nozzle and previously built layers[9]. Kalami et al.[10] encountered nozzle collision issues while building a dome structure and used the geometrical partitioning method for successful fabrication [10]. However, the transition region between the partitions shows large surface irregularities, which increases the roughness values significantly in these regions [11]. A combination of multi-directional segmentation and single-directional slicing was carried out by Xiangping et al. for building overhang structures [12].

Prahar et.al developed a novel slicing algorithm to tilt and rotate the build platform to avoid support structure using a robotics FDM setup[13].

Thus, the process methodology for building overhang structures using LDED is limited to geometrical partitioning or segmentation. The literature indicates that there are limited published works available on the development of tool paths for building overhang components such as dome structures in a single step. The present work proposes a novel approach based on identification of maximum allowable overhang angle and collision detection interactively to directly build the dome structures in a single step, which can pave way for building complex and lightweight components using LDED.

## 2. Experimental Details

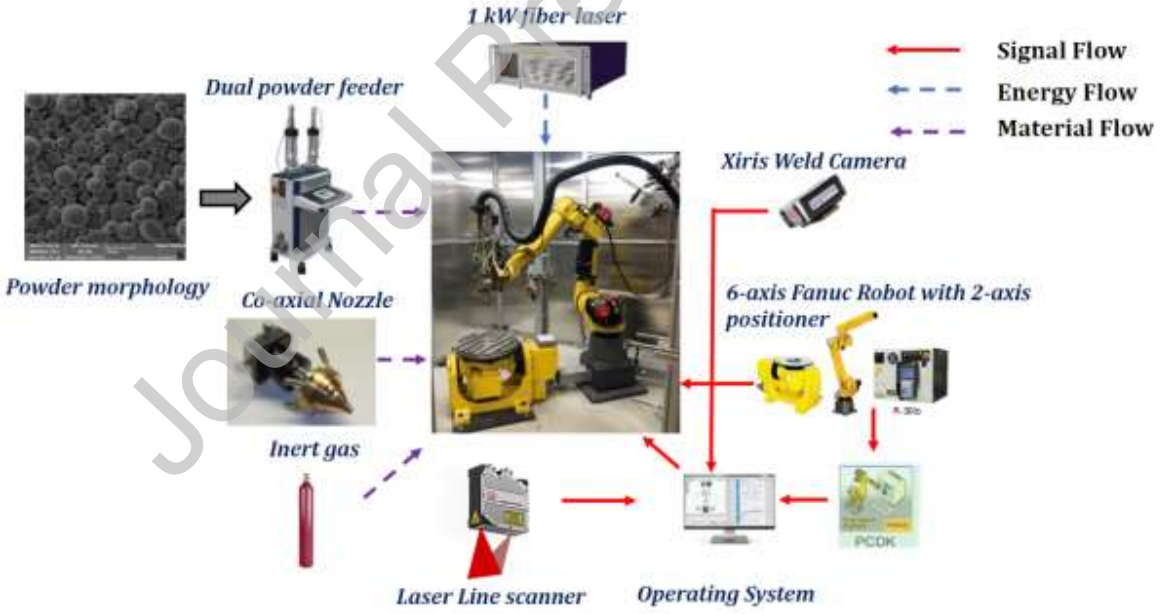


(a)

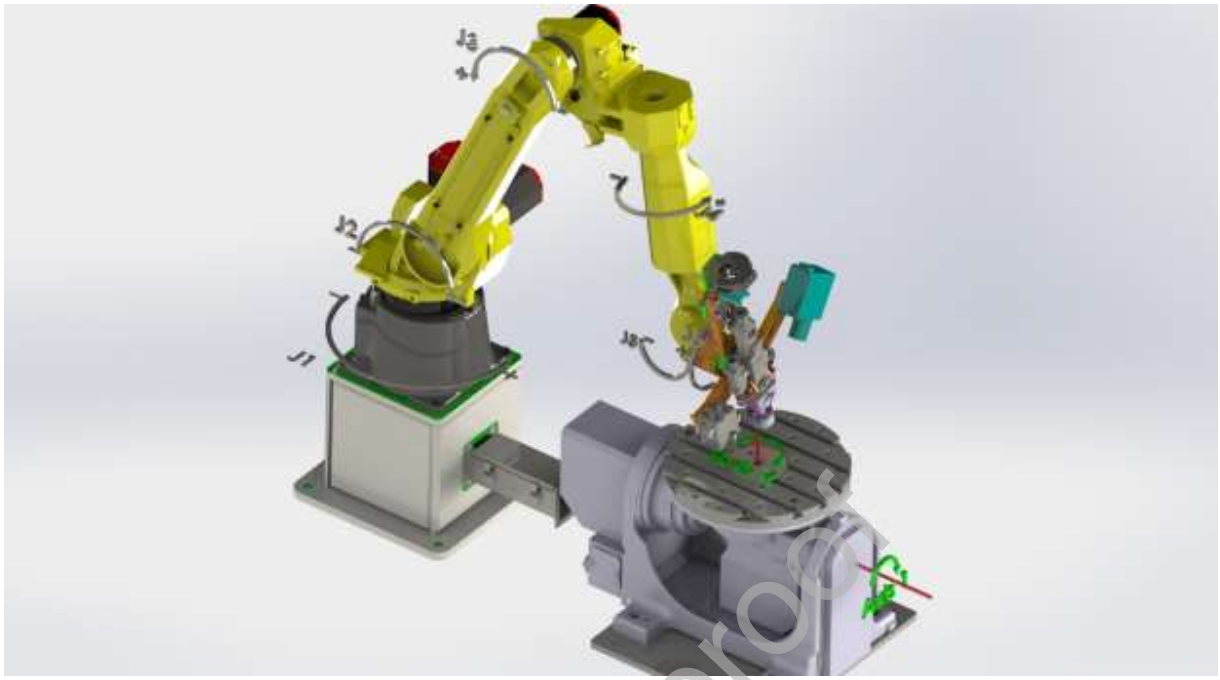


(b)

Figure 1: Schematic of the (a) LDED system (b) rotational axes of robot and the positioner

SS 316L powder of size 15 - 45 µm and spherical morphology (D10 = 19.66 µm, D50 = 29.54 µm, D90 = 44.08 µm), made by Carpenter Additive through gas atomization, was used as the feedstock material. An in-house developed 1 kW fiber laser-based robotic LDED system equipped with a dual hopper powder feeder and the co-axial nozzle was used for experiments as shown in Figure 1(a). A 6-axis Fanuc M-20iA robotic arm with 2-axis servo positioner H875 and a maximum payload of 500 kg was used for the deposition. The robot and the servo positioner are controlled by the R30iB controller. The robot and positioner rotation axis are shown in Figure 1(b). PROERA 3D CAD/CAM software was used for the tool-path planning. Argon gas at a flow rate of 10 lpm and 15 lpm were used as the carrier and shielding gas, respectively.

Initially, single-track experiments are carried out by varying laser powder, powder feed rate and scanning speed to identify process parameters for building thin-wall structures. The process parameter combination that yielded continuous deposition with requisite width (1.5 – 2 mm as per the wall thickness of cone and dome) and minimal dimensional deviation is selected for subsequent experiments. The process parameters selected for the study is shown in Table 1.

Table 1: Process parameters used for the study

| **Process parameter** | **Value** |
|---|---|
| Laser power | 640 W |
| Powder feed rate | 5 g/min |
| Scanning speed | 8 mm/sec |
| Laser spot diameter | 1.2 mm |

Initially, a set of experiments were conducted to find the $\alpha_{max}$ by building cones having base diameter and height of 20 mm and α varying from 0° - 40°with an interval of 5°. Further, the dome of radius 50 mm and thickness 2 mm was built using the developed methodology. The cross-section view of the dome CAD model is shown in Figure 2(a). LDED built dome was further scanned using a structured light optical scanner (Make: Hexagon, Model: AICON SmartScan). Figure 2 (b) presents the setup used for scanning the part using an optical scanner. The S-350 mm lens with a field of view of 260 × 205 mm was used for the scanning. The accuracy of the scanner is ±15 µm and the obtained point cloud of the dome includes ~ 1.2 million points. OptoCat 2018R3 software was used for data acquisition and triangulation accuracy of 0.005 mm was used to convert the point cloud to STL file. Subsequently, CAD model and the scanned model are imported in PolyWorks|Inspector™. Automatic alignment is

performed to align the two geometries together and to overlay the CAD model of the component with the scanned data. A CAD to the part comparison of the dome was carried out to identify the deviation from intended dimensions. In addition, the dome and cone structures are sectioned, mounted, polished using standard metallography procedure. The mirror-finished sample surface is observed using a digital microscope (Make: Keyence; Model: VK-X250) to check the presence of defects.


(a)

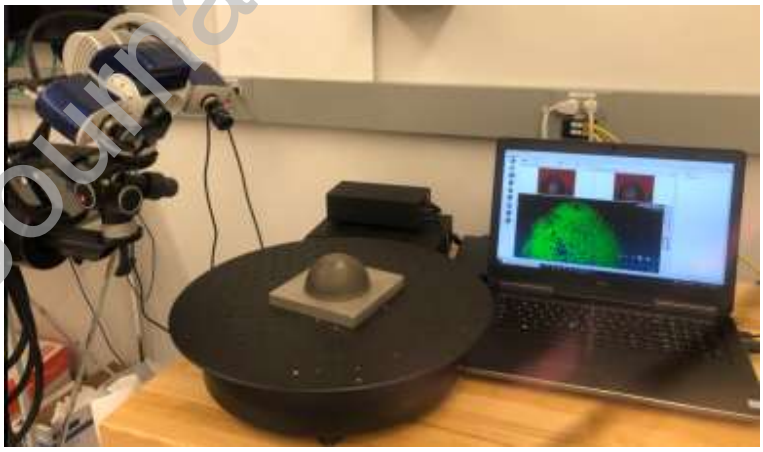

(b)

Figure 2: LDED built dome (a) Schematic (b) scanning using a structural light scanner

## 3. Developed Methodology for Dome Structures

LDED can take advantage of 5-axis techniques such as lean (tilt) and lead angles to avoid collision between the nozzle and the 3D printed parts. It must be considered that the lead angle must not exceed the αmax [10] as large values of α may result in lack of support for melt pool leading to melt pool collapse (see section 4). Lean (Tilt) angle is the orientation of the nozzle axis measured in the plane perpendicular to the deposition direction as shown in Figure *3*(a)[14], where D is the deposition (travel) direction, N is the substrate normal vector, and B is the Cross product of D and N. Lead angle is defined as the orientation of the nozzle axis measured in the plane parallel to the deposition (travel) direction as shown in Figure 3(b)[15] and it is measured from the perpendicular to the direction of deposition (travel). When the nozzle axis tilts in the B-N plane or to the side of the deposition (travel) direction, the angle is called lean (tilt) angle, and when the nozzle axis tilts in the D-N plane or forward and backward in the relation to the deposition (travel) direction, it is called lead angle.

To manufacture a dome in a single step using LDED, in this work, the tilt angle is used to avoid the collision between the nozzle and previously built material while keeping in mind that the tilt angle cannot exceed $\alpha_{max}$ [4]. In Figure 3(c), $\vec{b}$ is the deposition direction and $\overrightarrow{N_c}(p)$ is the surface normal direction to the surface at the point P. The relationship between the $\vec{b}$ and $\overrightarrow{N_c}(p)$ is $\overrightarrow{N_c}(p).\vec{b} = 0$ to ensure that the deposition can be supported fully by the previously built layers. However, due to partial support from previous layers, the deposition range can be extended as shown in Equation 1.

$$-\sin\alpha_{max} \leq \overrightarrow{N_c}(p).\vec{v} \leq 0 \quad (1)$$

where, $\alpha_{max}$ , a function of $\frac{\Delta d_{max}}{\Delta l}$ , is the maximum allowable overhang angle along the deposition direction of $\vec{b}$, $\Delta d_{max}$ is the maximum offset value that a new layer can overhang from the previous layer without melt pool collapse, and $\Delta l$ is the layer thickness.

Figures 3 (d) and 3 (e) presents the schematic indicating the variation in $\alpha$ in the dome and flowchart of the developed methodology, respectively. Initially, the geometry is prepared, which includes the creation of a surface model. Subsequently, the αmax is given as the input and the starting tilt angle is 0° in the beginning. The input track width and height are used to generate the stock model of the deposited material and the collision of the stock model versus the nozzle head is performed within the interface of PROERA 3D. If the collision is not detected, the toolpath will be generated in the robot native language. If the collision is detected (refer to Figure 3(f)), the tilt angle will be increased, and the toolpath will be re-generated. This continues until the methodology converges to the tilt angle that avoids the collision.

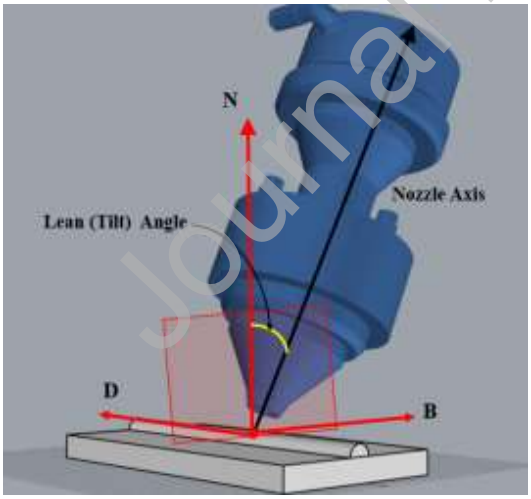


(a)

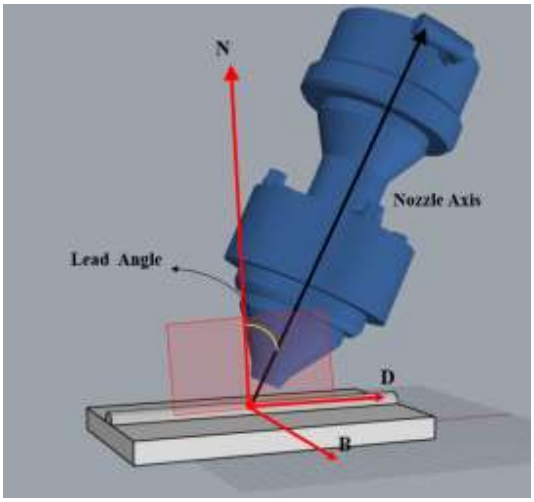


(b)

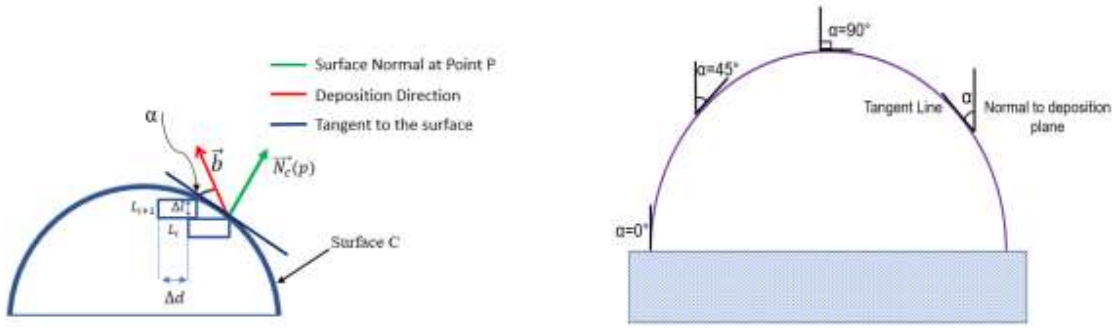


(c) (d)

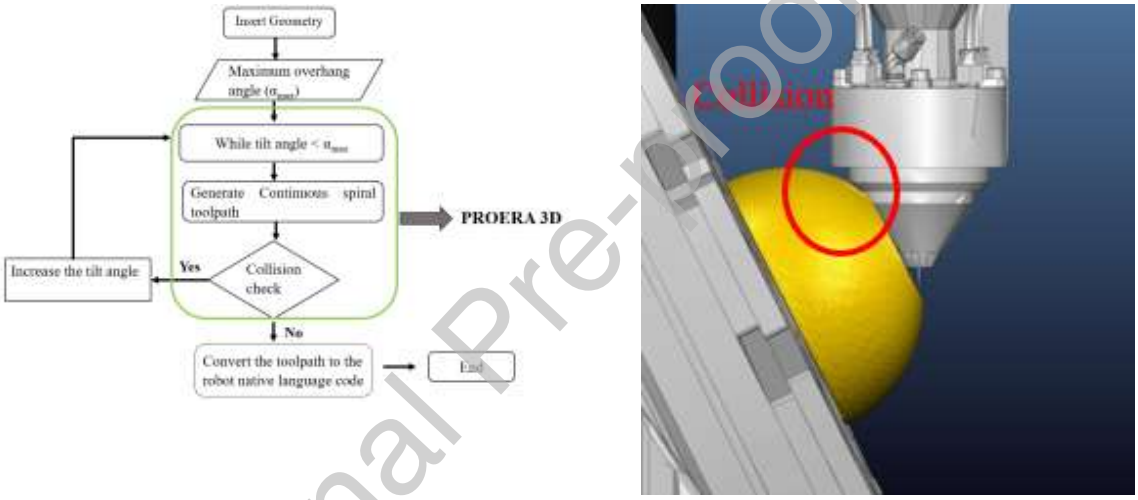


(e) (f)

Figure 3: Dome structure using LDED (a) lead angle schematic (b) lean angle schematic (c) (d) Varying α for a typical dome (e) algorithm (f) collision issue

## 4. Results and Discussion

Figure *4*(a) and Figure *4*(b) presents the schematic of the overhang structures and photographic view of built cones, respectively. The overhang cone geometry was built by laying overlapped tracks one over the other, while the nozzle orientation remains normal to the substrate. As discussed in the previous section, the primary data for developing the methodology is the $\alpha_{max}$. It was observed the $\alpha_{max}$ of 35° can be used to build cone structures of height 20 mm without the

material collapse as the melt pool becomes asymmetrical and collapses when the $\alpha$ exceeds 35º. This can be mainly due to the imbalance between the gravitational forces, viscous forces, and surface tension. The 35º will result in an offset value of 0.4 mm as per Equation (2) based on the nominal track height and a track width of 0.5 mm and 1.5 mm, respectively (obtained from process parameter setting).

$$\tan \alpha_{max} = \frac{\Delta d}{\Delta l} \quad (2)$$

Figure 4(c) presents the cross-sectional images of cones built with 5-degree, 20 degree, and 35 degree overhang angle. It is observed that the built structures are crack-free and micro-pores are mainly seen along the cross-section. The micro-pores are primarily spherical, with the presence of a few irregular pores. The spherical and irregular pores are mainly due to gas-porosity and lack-of-fusion porosity, respectively. Gas porosity is generated primarily due to gas entrapment inside the melt-pool during solidification. It can also be due to the presence of porosity inside the powder particles, which are generated during powder manufacturing. These pores get transferred to the built part during the fabrication. On the other hand, a lack of fusion porosity is generated due to the insufficient bonding at isolated locations due to insufficient heat input and/or unexpected disturbances during LDED. An increase in the number of lack of fusion pores are seen with increase in overhang angle, which is primarily due to increase in the melt-pool instability at higher overhang angles [16-17]

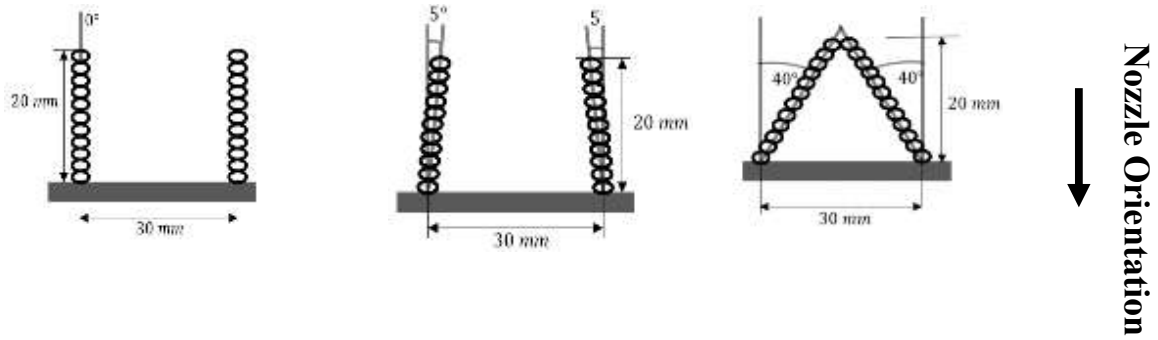


(a)

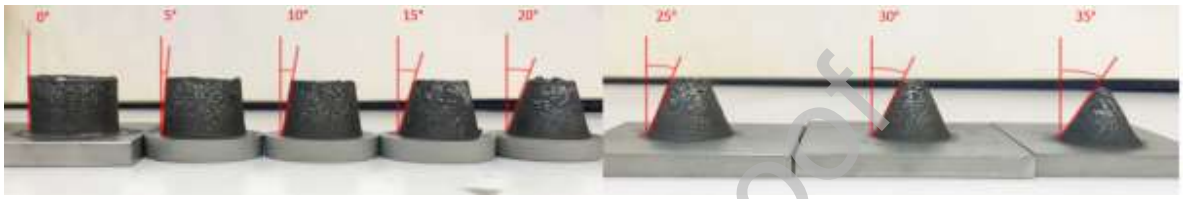


(b)

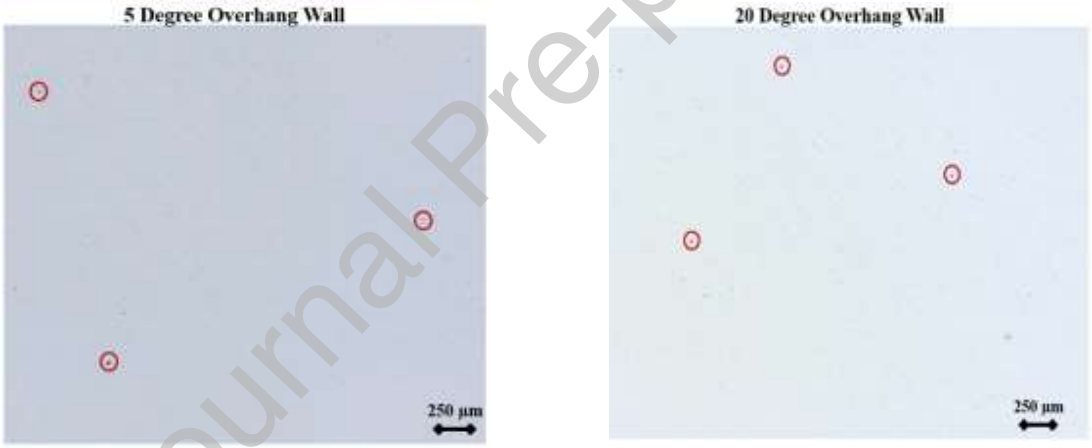

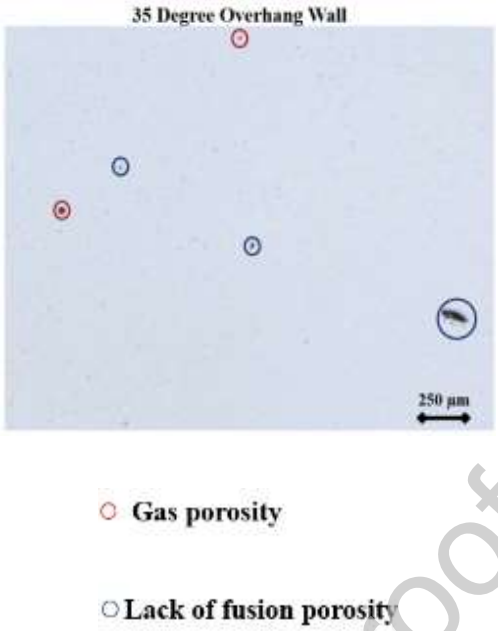


(c)

Figure 4*:* LDED of overhang structures (a) Schematic (b) photographic view (c) cross-sectional images

Further, the deposition is simulated (refer to Figure *5* (a)) and carried out as per the required machine configuration (refer to Figure *5*(b)). The algorithm verifies that a tilt angle of 32.5º will be suitable to build the dome using the rotary setup. Further, the angle is transferred from the tilt angle to the tilt angle of the rotary table. The orientation of the nozzle is perpendicular to the previously built layer up to 57.5º and the tilting start at this point. The $\alpha$ varies from 0 to 32.5º from the bottom layers to the top of the dome as shown in Figure *5*(c). $\alpha_1$, $\alpha_2$ , and $\alpha_3$ shows the angle between the normal to the previous layer direction and the nozzle at different curvature angles in the dome at different positions. For the initial layers, $\alpha_1$ is 90º indicating that the nozzle is normal to the previously built layer, while at the top layers $\alpha_3$ is 57.5º and the corresponding $\alpha$ at the top of the dome is equal to $\beta_3$ (Maximum tilt angle), which is equal to

32.5º. Figure 5(d) presents the photographic view of the built dome structure and it can be seen that deposition is uniform with reduced surface irregularities as opposed to ones built with partitioning [10]. A comparison with the CAD model (refer to Figure 6(b)) shows the uniform surface quality and good agreement with the intended dimensions. The deviation is lower than 0.5 mm at the lower to middle layers and the maximum deviation of ~ 1.5 - 2 mm (about 2% of the dome diameter) is observed at the top layers primarily due to the higher degree of overhang.

Figure 6 (a) shows the typical overlay of the CAD model cross section and the scanned data cross section. It is observed that the maximum deviation is at the top of the dome printed with maximum overhang angles of 32.5 degrees.

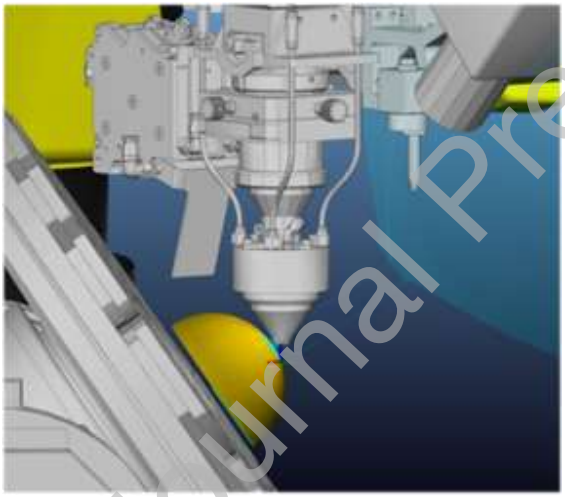

(a)

(b)

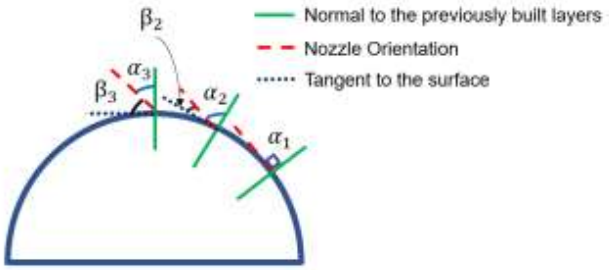


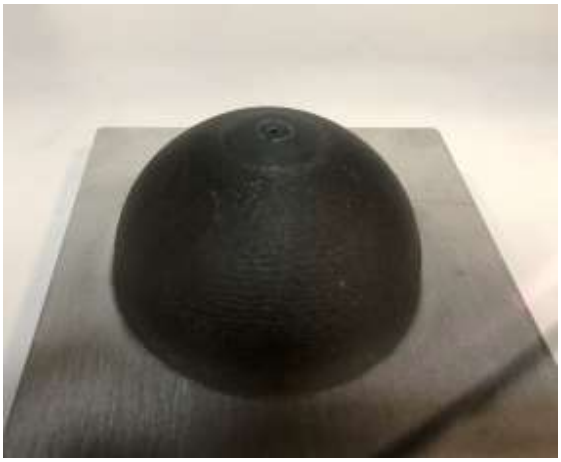

(c) (d)

Figure 5: LDED of dome structures (a) simulation (b) deposition process (c) schematic of varying overhang and tilt angle (d) final part

CAD Model

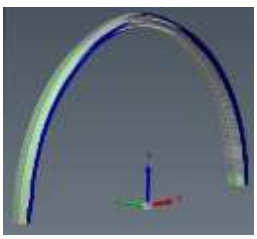

Scan Model

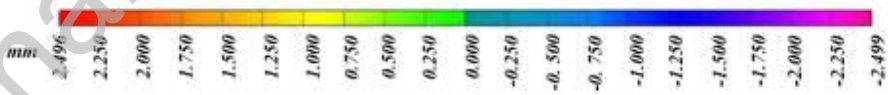


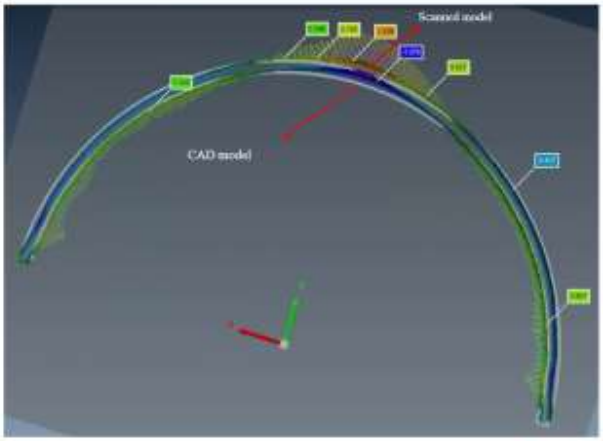


All dimensions are in mm

(a)

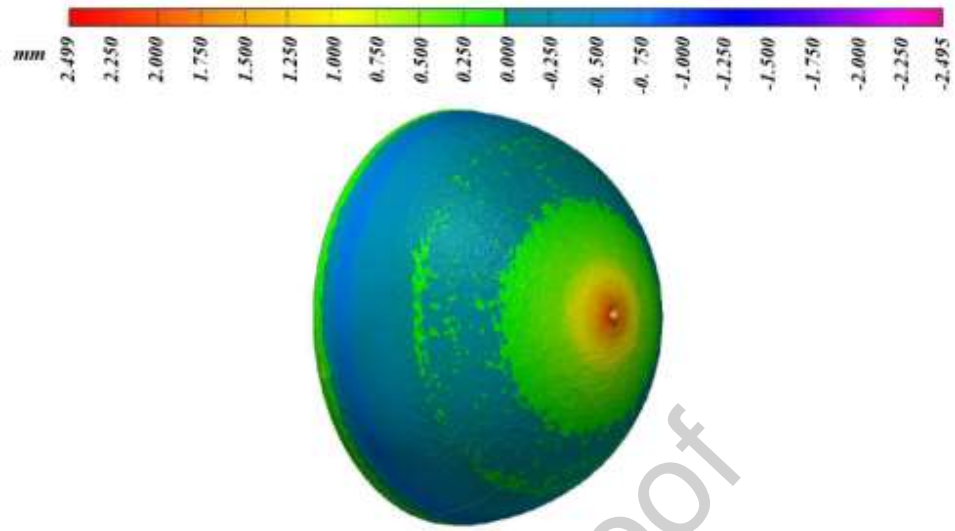


(b)

Figure 6: CAD to part comparison of (a) typical cross-section (b) full dome structure

Figure *7*(a) presents the microscopic images obtained from different locations of the built dome structure. It is observed from Figure *7*(a) that the deposition is defect-free without cracks and macro scale porosity. However, a deeper investigation of the structures shows that micro-porosity is seen at different locations as shown in Figure *7* (b). The micro-pores are mainly gas porosities, with the presence of a few lack of fusion pores at isolated locations.

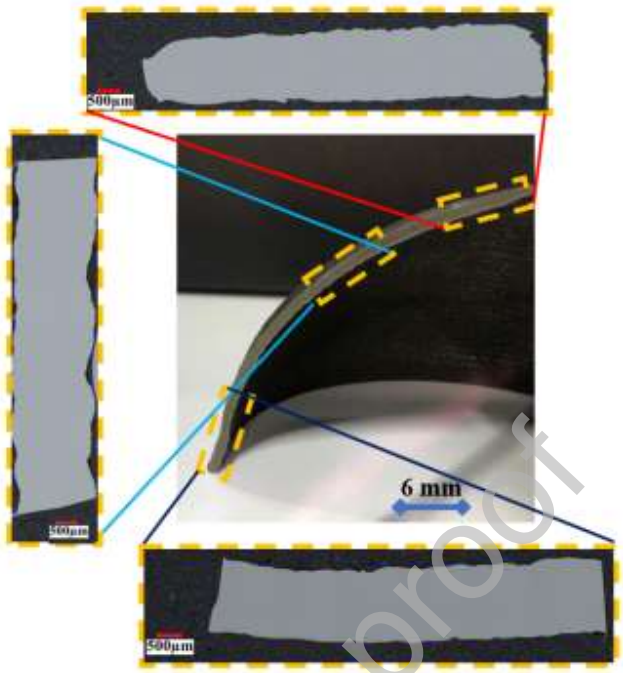


(a)

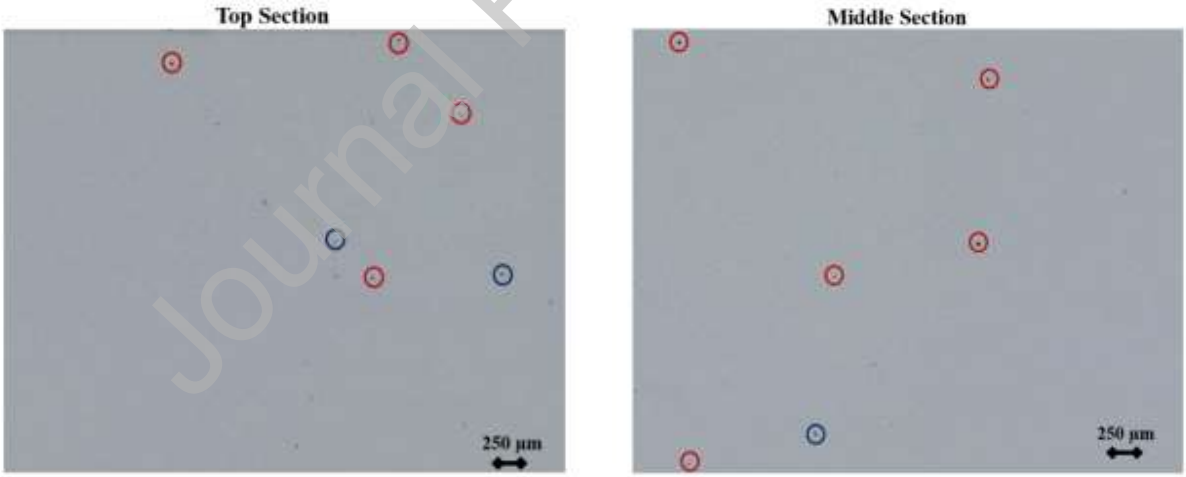

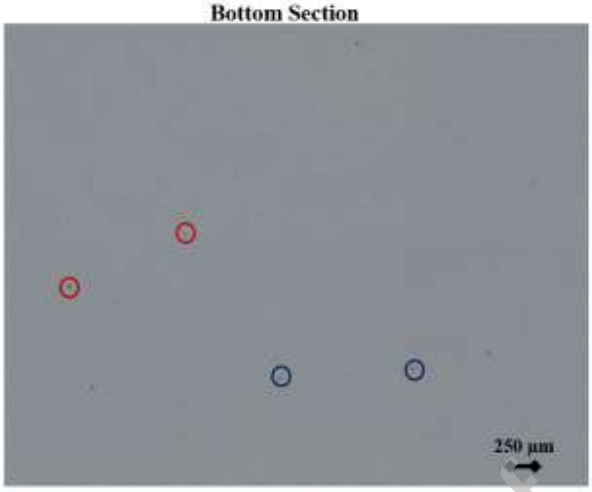


(b)

Figure 7: Cross-sectional images of the dome at different locations (a) lower magnification (b) higher magnification

## 5. Conclusions

The present work proposes a novel methodology to manufacture the parts with variable overhanging angle. The methodology aids to avoid collision between the nozzle and the previously built layers while providing a proper melt pool stability, which allows the fabrication of the dome in a single step. Further, the methodology is verified by manufacturing the part and CAD to part comparison shows the maximum deviation of 2% with respect to the diameter of the original CAD model data. The proposed methodology avoids partitioning of the component and the deployment of computationally expensive algorithms to manufacture overhang dome structures using LDED. The study will be further extended to the evaluation of different particle size distribution, and materials on the overhang geometries. In addition, the evaluation of structural integrity and the evolution of the microstructure of the fabricated dome component will also be carried out in the future works. The study will also be extended by deploying

adaptive trajectory planning to improve the dimensional accuracy of the dome. The study will pave a way for fabricating thin-walled storage tanks for various engineering applications.

**Acknowledgement**

This work is supported by Federal development of Ontario (Fed-Dev) and Promation Engineering. The authors would like to thank Ali Zardoshtian and Henry Ma of MSAM, University of Waterloo for powder characterization, optical scanning and microscopic analysis.

**References**

[1] W. L. Ng, C. K. Chua, and Y.-F. Shen, "Print Me An Organ! Why We Are Not There Yet," *Prog. Polym. Sci.*, vol. 97, p. 101145, 2019, doi: https://doi.org/10.1016/j.progpolymsci.2019.101145.

[2] H. W. Tan, J. An, C. K. Chua, and T. Tran, "Metallic nanoparticle inks for 3D printing of electronics," *Adv. Electron. Mater.*, vol. 5, no. 5, p. 1800831, 2019.

[3] Y. Y. C. Choong, S. Maleksaeedi, H. Eng, S. Yu, J. Wei, and P.-C. Su, "High speed 4D printing of shape memory polymers with nanosilica," *Appl. Mater. Today*, vol. 18, p. 100515, 2020, doi: https://doi.org/10.1016/j.apmt.2019.100515.

[4] Y. Ding, R. Dwivedi, and R. Kovacevic, "Process planning for 8-axis robotized laser-based direct metal deposition system: A case on building revolved part," *Robot. Comput. Integr. Manuf.*, 2017, doi: 10.1016/j.rcim.2016.08.008.

[5] N. Chen and M. Frank, "Process planning for hybrid additive and subtractive manufacturing to integrate machining and directed energy deposition," 2019, doi: 10.1016/j.promfg.2019.06.140.

[6] P. Kulkarni, A. Marsan, and D. Dutta, "A review of process planning techniques in layered manufacturing," *Rapid Prototyp. J.*, vol. 6, no. 1, pp. 18–35, 2000.

[7] J. Jiang, S. T. Newman, and R. Y. Zhong, "A review of multiple degrees of freedom for additive manufacturing machines," *Int. J. Comput. Integr. Manuf.*, vol. 34, no. 2, pp. 195–211, Feb. 2021, doi: 10.1080/0951192X.2020.1858510.

[8] J. Jiang, J. Stringer, X. Xu, and R. Y. Zhong, "Investigation of printable threshold overhang angle in extrusion-based additive manufacturing for reducing support waste," *Int. J. Comput. Integr. Manuf.*, vol. 31, no. 10, pp. 961–969, Oct. 2018, doi: 10.1080/0951192X.2018.1466398.

[9] P. M. Bhatt, R. K. Malhan, A. V Shembekar, Y. J. Yoon, and S. K. Gupta, "Expanding capabilities of additive manufacturing through use of robotics technologies: A survey," *Addit. Manuf.*, vol. 31, p. 100933, 2020, doi:

https://doi.org/10.1016/j.addma.2019.100933.

[10] H. Kalami and J. Urbanic, “Process Planning of Creating a Surface Dome with Bead Deposition Additive Manufacturing,” 2019, doi: 10.1016/j.ifacol.2019.10.069.

[11] H. Kalami and J. Urbanic, “Exploration of surface roughness measurement solutions for additive manufactured components built by multi-axis tool paths,” *Addit. Manuf.*, vol. 38, no. August 2020, p. 101822, 2021, doi: 10.1016/j.addma.2020.101822.

[12] W. Xiangping, Z. Haiou, W. Guilan, and W. Lingpeng, “Adaptive slicing for multi-axis hybrid plasma deposition and milling,” 2014.

[13] P. M. Bhatt, R. K. Malhan, P. Rajendran, and S. K. Gupta, “Building free-form thin shell parts using supportless extrusion-based additive manufacturing,” *Addit. Manuf.*, vol. 32, p. 101003, 2020, doi: https://doi.org/10.1016/j.addma.2019.101003.

[14] “Lead/Lean Angles,” 2020. https://knowledge.autodesk.com/support/powermill/learn-explore/caas/CloudHelp/cloudhelp/2018/ENU/PWRM-ReferenceHelp/files/GUID-E3341040-E6FD-400F-A71F-6AE3BCF7147D-htm.html (accessed Jan. 26, 2022).

[15] M. Fujiki, J. Ni, and A. J. Shih, “Tool Path Planning for Near-Dry EDM Milling With Lead Angle on Curved Surfaces,” *J. Manuf. Sci. Eng.*, vol. 133, no. 5, Sep. 2011, doi: 10.1115/1.4004865.

[16] S. Bakhshivash *et al.*, “Printability and microstructural evolution of Ti-5553 alloy fabricated by modulated laser powder bed fusion,” *The International Journal of Advanced Manufacturing Technology*, 2020. .

[17] T. DebRoy *et al.*, “Additive manufacturing of metallic components – Process, structure and properties,” *Progress in Materials Science*, 2020. .

**Declaration of interests**

☒ The authors declare that they have no known competing financial interests or personal relationships that could have appeared to influence the work reported in this paper.

☐The authors declare the following financial interests/personal relationships which may be considered as potential competing interests: